Hall Barrientos, Ivan J., Paladino, Eleonora, Brozio, Sarah, Passarelli, Melissa K., Moug, Susan, Black, Richard A., Wilson, Clive G. and Lamprou, Dimitrios A. (2016) *Fabrication and characterisation of drug-loaded electrospun polymeric nanofibers for controlled release in hernia repair.* International Journal of Pharmaceutics, 517 (1-2). pp. 329-337. ISSN 0378-5173.

The version of record is available from
https://doi.org/10.1016/j.ijpharm.2016.12.022

This document version
Author's Accepted Manuscript

DOI for this version

International Journal of Pharmaceutics

Fabrication and characterisation of drug-loaded electrospun polymeric nanofibers for controlled release in hernia repair

Ivan J. Hall Barrientos[1,2], Eleonora Paladino[2,3,4], Sarah Brozio[2], Melissa K. Passarelli[4], Susan Moug[5], Richard A. Black[1], Clive G. Wilson[2], Dimitrios A. Lamprou[2,6*]

[1] Biomedical Engineering, University of Strathclyde, Glasgow, United Kingdom

[2]Strathclyde Institute of Pharmacy and Biomedical Sciences (SIPBS), University of Strathclyde, 161 Cathedral Street, Glasgow, G4 0RE, United Kingdom

[3]EPSRC Centre for Innovative Manufacturing in Continuous Manufacturing and Crystallisation (CMAC), University of Strathclyde, Technology and Innovation Centre, 99 George Street, G1 1RD Glasgow, United Kingdom

[4]National Physical Laboratory (NPL), Hampton Road, Teddington, Middlesex, TW11 0LW, United Kingdom

[5]National Health Service (NHS), Royal Alexandra Hospital, Paisley, PA2 9PN, United Kingdom

[6]Medway School of Pharmacy, University of Kent, Medway Campus, Anson Building, Central Avenue, Chatham Maritime, Chatham, Kent, ME4 4TB, United Kingdom

* Corresponding author. E-mail address: d.lamprou@kent.ac.uk, Tel.: +441415484968

Abstract

The chemical distribution and mechanical effects of drug compounds in loaded electrospun scaffolds, a potential material for hernia repair mesh, were characterised and the efficacy of the material was evaluated. Polycaprolactone electrospun fibres were loaded with either the antibacterial agent, irgasan, or the broad-spectrum antibiotic, levofloxacin. The samples were subsequently characterised by rheological studies, scanning electron microscopy (SEM), atomic force microscopy (AFM), contact angle goniometry (CAG), *in vitro* drug release studies, antibacterial studies and time-of-flight secondary ion mass spectrometry (ToF-SIMS). Increased linear viscoelastic regions observed in the rheometry studies suggest that both irgasan and levofloxacin alter the internal structure of the native polymeric matrix. *In vitro* drug release studies from the loaded polymeric matrix showed significant differences in release rates for the two drug compounds under investigation. Irgasan showed sustained release, most likely driven by molecular diffusion through the scaffold. Conversely, levofloxacin exhibited a burst release profile indicative of phase separation at the edge of the fibres. Two scaffold types successfully inhibited bacterial growth when tested with strains of *E. coli* and *S. aureus*. Electrospinning drug-loaded polyester fibres is an alternative, feasible and effective method for fabricating non-woven fibrous meshes for controlled release in hernia repair.

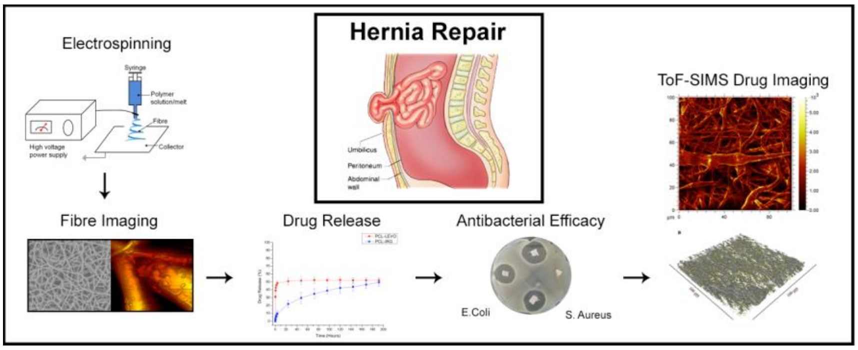

Keywords: Electrospinning, Scaffolds, Hernia, Drug Release, Physicochemical Characterisation.

1. Introduction

Hernia repair, one of the most common general surgeries performed, is complicated by bacterial infections and implant rejection [1]. Commercially available mesh devices currently employed in hernia repairs contain brained or knitted fibres. The mechanical properties of the mesh and the biocompatibility of the material are critical to the healing process. Tissue incorporation, a key factor in the success of the graft device is dependent on the material type, density, compliance and electrical properties of the mesh [2]. Graft failure motivates research into new fabrication methods for incorporating biomaterials and drug encapsulation in novel mesh matrices, such as hot-melt extrusion [3], electrospinning [4], 3D printing [5] and high-speed rotary spinning [6].

Electrospinning is the most popular and preferred technique for nanofiber fabrication due to its simplicity, cost-effectiveness, flexibility, and ability to spin a broad range of polymers [7]. The method allows for the simple and direct functionalization of fibres with drug compounds and is compatible with solvents such as chloroform and dimethyl sulfoxide. In addition, the process of electrospinning with the use of solvents such as chloroform, dimethyl sulfoxide etc., allows functionalisation of the scaffolds through the inclusion of drugs in the polymer-solvent solution without the need for a complicated preparation process [8]. Electrospinning has previously been applied to the fabrication of triclosan/cyclodextrin inclusion complexes [9], the construction of scaffolds with perlecan domain IV peptides [10], manufacture of biocatalytic protein membranes [11], and encapsulation of levofloxacin in mesoporous silica nanoparticles [12]. Given the broad applications of electrospinning, there has been previous research specifically focused on the development of electrospun polymeric materials for hernia repair mesh devices. Electrospinning produces scaffolds containing micro-fibres and this is an advantageous feature not observed in braided mesh commercial devices – these microfibers also introduce mechanical anisotropy and provide topographic features to guide cell alignment [13]. However, electrospun fibres typically incorporate the use of organic solvents and for applications such as hernia repair or tissue engineering, the toxicity of organic solvents used could be highly critical – avoiding organic solvents is of outmost importance for applications in medicine and pharmacy [14], [15].

The purpose of this study is to examine the physicochemical properties, bacteria response, and drug loading of electrospun scaffolds. The polymer chosen for this study is *polycaprolactone* (PCL); a biodegradable polyester commonly used in biomedical applications for controlled release and targeted drug delivery [16]. PCL, a biodegradable aliphatic polyester [17], is an obvious candidate for drug delivery systems due to its high biocompatibility and ease of degradation in the human body [18]. Drug loading of structures that mechanically resemble interfacial tissue and which allows short or long-term release of suitable bioactives may be utilisable in hernia-repair meshes. PCL was chosen in this research as it has a high permeability to a variety of drug molecules (e.g. gentamycin, chitosan) and low toxicity [19]. The matrix was loaded and electrospun with two drugs, *irgasan* (an antibacterial agent used commonly in soaps, detergents and surgical cleaning agents) or *levofloxacin* (a broad-spectrum antibiotic used commonly to treat gastrointestinal infections). The mechanical characteristics, morphology, surface hydrophobicity, drug efficacy and chemical distribution were characterised with an array of analytical techniques. The results from this study should help to build platform to aid future work with various fabrication methods, such as extrusion and shaping using 3D printing.

2. Materials & Methods

2.1 Materials

Polycaprolactone (PCL) with a mean molecular weight of 80 kD, Irgasan (variation of Triclosan, >97%), Levofloxacin (>98%), and all the solvents used for the electrospinning were obtained from Sigma Aldrich. The solvents consisting of chloroform (anhydrous, containing amylenes as stabilizers, >99%) and N,N-dimethylformamide (DMF, anhydrous 99.8%).

2.2 Preparation of PCL Solutions

Different solutions with a polymer concentration of 12% (w/w) were prepared to be used within the electrospinning method – this particular concentration was used due to its possessed suture retention and tensile strengths appropriate for hernia repair, as specified for similar electrospun scaffolds described by Ebersole *et al* [20]. Various PCL formulations were constructed of a total weight of 25 g per solution, which allowed for PCL (12% w/w) and a 9:1 (w/w) ratio of chloroform (CLF) to N,N-dimethylformamide (DMF). For the unloaded polymer solution, 3 g of PCL was dissolved in 22 g of CLF:DMF (9:1) which was initially mixed through 30 min in a centrifuge, a further 30 min in a sonicator (Elma S30 Elmasonic) and a final 1 h with a magnetic stirrer. This process was vital to ensure that the solution was fully homogeneous. The solution was left overnight, and a further 30 min of sonication applied the following morning in order to confirm the homogeneity of the solution. For the irgasan-loaded solutions, the same method was applied, except the solution contained 1% (w/w) irgasan. The concentration of the levofloxacin-loaded solutions was 0.5% (w/w), providing sufficient sensitivity in the release cell for accurate UV analysis. All the preparations turned to clear solutions. These observations were interpreted to determine that the solutions had successfully homogenised. The solutions were then subsequently used in the electrospinning process and for rheological analysis.

2.3 Electrospinning of PCL Solutions

The PCL test specimens were fabricated for each polymeric solution, using a custom in-house electrospinning apparatus, which consisted of a syringe pump (Harvard Apparatus PHD 2000 infusion, US) and two 30kV high-voltage power supplies (Alpha III series, Brandenburg, UK). The polymer solution was loaded into glass syringe and fed through tubing with a metal needle tip attached at the end. The needle was clamped into place, to allow a high-voltage supply to run through it, which allowed an electric field to be created between the needle and the target plate. The syringe was clamped to a pump, which determined the specific injection flow rate of the polymeric solutions. For each of the three solutions (e.g. unloaded, irgasan-loaded, and levofloxacin-loaded), 3 varying flow rates of 0.5, 1 and 1.5 ml h^{-1} were applied across varying voltages of 2 kV – 5 kV (needle) and 10 kV – 18 kV (target plate). The variation in flow rate and applied voltages was to correct any problems that occurred during fabrication, i.e. ‘spitting’ of solution at the target plate, or any potential beading (which was examined through SEM). The fabrication of this solution was electrospun onto the target that was covered with aluminium foil, in order for the final material to be removed and used for further characterisation. The final yield of electrospun PCL resulted in thin, flexible sheets of material.

2.4 Rheological Studies

A Thermo Scientific HAAKE MARS II rheometer with a P35 TiL cone and plate was used to measure the rheological and mechanical behaviour of the different unloaded and loaded polymeric solutions. The objective of this experiment was to examine the viscoelastic properties of the PCL solution, specifically to determine whether the irgasan or levofloxacin is having an effect on the mechanical properties of the polymer. The method used was taken and modified from the rheological study undertaken by Bubel *et al* [15]. In briefly, an oscillating amplitude sweep between 0.1 Pa – 1000 Pa at a frequency of 1 Hz was used to determine the linear viscoelastic region (LVER) of the samples. Once the LVER is determined from the amplitude sweep, a downwards oscillating frequency sweep from 10 Hz – 0.1 Hz with a shear stress (Pa) within the LVER was then used in order to help understand the nature of the solutions concerning strength and stability. The experiments were repeated 4 times per solution, and for each experiment, each data point (20 data points per method) was optimised to repeat each measurement 5 times.

2.5 Scanning Electron Microscopy (SEM)

The morphology and diameter of individual fibres spun from PCL solution were determined from scanning electron micrographs of each sample (TM-1000, Hitachi, UK, Ltd.). The samples were mounted on an aluminium plate with conductive tape. Images of fibres were taken at various locations of each electrospun PCL scaffold in order to determine the overall uniformity of fibres. Prior to imaging, the samples were sputter coated with gold for 30 sec using a Leica EM ACE200 vacuum coater, the process being repeated four times in order to increase the conductivity of the samples.

2.6 Atomic Force Microscopy (AFM)

Further morphological analysis was undertaken through atomic force microscopy. A Multimode 8 microscope (Bruker, USA), with Scanasyst-Air probes (Bruker, USA) was used in Peak Force Quantitative Nano Mechanics (QNM) mode, as described by Lamprou *et al* [21]. The imaging of the fibres was performed under ambient conditions, with a silicon cantilever probe. The tip radius of the probe and the spring constant were calculated to be in the regions of 0.964 nm (18° tip half angle) and 0.4935 N/m, respectively. The scan sizes ranged from 200 nm to 25 µm, at a scan rate of 0.977 Hz with 256-sample resolution. The Roughness Average (Ra) values were determined by entering surface scanning data, and digital levelling algorithm values were determined using Nanoscope Analysis software V1.40 (Bruker USA). AFM images were collected from two different samples and at random spot surface sampling.

2.7 Contact Angle Goniometry (CAG)

To monitor changes in wettability of the scaffolds, sessile drop contact angle for distilled water was measured by contact angle goniometry, using a contact angle goniometer (Kruss G30, Germany) as described by Lamprou *et al* [22].

2.8 In Vitro Drug Release Studies

The drug releases of the irgasan/levofloxacin loaded PCL scaffolds were measured in order to determine the release profile of the drugs. Samples of PCL-IRG were immersed in phosphate buffered saline (PBS) containing 0.5% sodium dodecyl sulfate (SDS) at 37 °C, and samples of PCL-LEVO were immersed in PBS only at 37 °C. This release study was based on the method cited by Duan *et al* [23]. The solutions were agitated using a shaker at a rate of 80 rev/min. The UV absorbance of both drugs was measured: irgasan at 280 nm [24], and levofloxacin at 292 nm [25] respectively. Measurements were taken at intervals at 15 min, 30 min, 1 h, 2 h, 4 h, 8 h, 24 hrs and every day after the 24 h mark for up to 7 days. At each point, 4 ml of solution was taken from the vial and replaced with fresh in order to satisfy the perfect-sink conditions and keeping the volume of the solution constant.

2.9 Antibacterial Studies

The antibacterial efficacy of the drug loaded electrospun scaffolds were tested against *Escherichia coli* (*E. coli*) 8739 and *Staphylococcus aureus* (*S. aureus*) 29213. *S. aureus* is Gram positive, *E. coli* is Gram negative and both bacteria are common causes of nosocomial infections. . Both irgasan and levofloxacin should have antibacterial effects. For this study, an agar diffusion method was used. Luria-Bertani (LB) agar was prepared from a formulation of 5 g tryptone, 2.5 g yeast extract, 5 g NaCl in 475 ml of deionized water. The LB agar was autoclaved and poured into 20ml plates. The *E. coli* and *S. aureus* were grown overnight in 5 ml of LB Broth, with both bacteria inoculated from a single colony. 150 µL of the *E. coli* and *S. aureus* cultures were spread onto six different plates of LB agar. Three plates consisted of spread *E. coli*, including a scaffold free plate, which acted as a control – the other 2 plates, were divided into 4 sections, with 1 section containing an unloaded PCL scaffold, and the other 3 containing PCL-irgasan and PCL-levofloxacin scaffolds. This procedure was repeated for three plates of spread *S. aureus*. The plates were incubated for 24 h, and subsequently examined. Diameters of the zones of growth inhibition were measured, and these data compared across the drugs and bacterial strains. This method was based on the method described by Davachi *et al* [26].

2.10 Time of Flight Secondary Ion Mass Spectrometry (ToF-SIMS)

ToF-SIMS data was acquired using a ToF-SIMS V mass spectrometer (ION-TOF GmbH, Münster, Germany) based at the Wolfson Foundation Pharmaceutical Surfaces Laboratory at the University of Strathclyde. The instrument is equipped with a bismuth liquid metal ion gun (LMIG), an argon gas cluster ion beam (GCIB) and a gridless reflectron time-of-flight mass analyzer.

Three different acquisition modes, detailed below, were used to analyse the fibres: high mass resolution spectroscopy, depth profiling, high lateral resolution imaging. Owing to the insulative nature of the materials, a low-energy electron beam (21 V) was used to compensate for charging.

2.10.1 High Mass Resolution Spectroscopy

For an optimal mass resolution, the primary ion beam (Bi_3^{++} primary ions) was pulsed at 10 kHz frequency with a pulse width of 17.0 ns. The primary ion gun energy was set at 30 kV and the pulsed target current was approximately 0.63 pA. Data was collected both in the positive and in the negative secondary ion polarities, in three replicates; each acquisition was made from different areas of the samples used in this study. The analysed area and the acquisition time, for each repetition, were respectively 100 µm × 100 µm and 120 seconds, delivering a primary ion dose density (PIDD) of approximately 4.6×10^{12} (primary ions/cm^2). Reference spectra for pure Levofloxacin and Irgasan compounds were acquired in positive and negative ion mode from 0 to 400 Da.

2.10.2 High Lateral Resolution Imaging

The LMIG was operated using the imaging mode, with high lateral resolution, and Bi_3^{++} was selected as primary ion beam. The primary ion gun energy was 30 kV and the pulsed target current was approximately 0.048 pA. High lateral resolution ion images were collected over a surface area of 100 µm × 100 µm, using a pulsed analysis beam (pulse width = 100 ns). The resolution was 256 × 256 pixels per image (pixel width was circa 0.4 µm). Each image was obtained with a final ion dose of 6.5×10^{12} primary ions/cm^2 or less. The dose was kept below the static limit of 10^{13} primary ions/cm^2 to minimize surface damages during the analysis. The images were processed with the ION-TOF SurfaceLab 6.6 software (Münster, Germany).

2.10.3 3D Imaging

The LMIG and the GCIB were employed in a dual-beam configuration to collect the depth profile and the 3D image data. The LMIG was operated in pulsed mode to investigate the lateral distribution of chemical species, while the Argon source was operated in DC mode to remove multiple layers of material from the sample surface between the analytical cycles. For the depth profiling analysis, the dual beam experiment used a 30 kV Bi_3^{++} primary ion beam for analysis and a 10 kV Ar_{1500}^{+} beam for sputtering. The pulsed current of the Bi_3^{++} primary ion beam was 0.048 pA and the DC current of the cluster Ar_{1500}^{+} was 10.22 nA, with a 500 seconds analysis time and 4 seconds sputtering time. The raster areas of the pulsed analysis beams and the DC sputter were 100 µm × 100 µm and 300 µm × 300 µm, respectively. The resolution was 256 × 256 pixels per image (pixel width of about 0,4 µm). Data was collected in the negative secondary ion mode. In the course of each acquisition, mass spectral information at each image pixel was collected in the m/z range of 0-917 m/z.

2.11 Statistical Analysis

All experiments were performed in triplicate with calculation of means and standard deviations. Two-way analysis of variance (ANOVA) was used for multiple comparisons along with Tukey's multiple comparing tests, followed by T-test to access statistical significance for paired comparisons. Significance was acknowledged for p values lower than 0.05.

3. Results and discussion

3.1 Rheological Studies

For each polymeric solution, multiple amplitude sweeps were used in order to correctly identify the linear viscoelastic region (LVR). This was repeated to detect any major variations in the LVR, and for a more accurate shear stress to be used in the frequency sweeps. For each of the samples, elastic modulus (G'), viscous modulus (G'') and shear viscosity (η) was calculated and subsequently analysed.

It can be seen in figure 1 that for all three solutions, the viscosity modulus (from 30 Pa to 80 Pa) is considerably greater than the elastic modulus (0.5 Pa to 6 Pa) which implies that the solutions exhibit significantly less elastic properties. As observed in figure 1c, both polymer-drug-loaded solutions of irgasan and levofloxacin show differences in the shear viscosity (η). The amplitude sweep demonstrated that these drugs caused a reduction in all three of these parameters – this may be caused by the possible transition from semi-dilute to dilute regime, where there are less polymer chain entanglements [27]. It is also worth noting that the LVR for the drug-loaded solutions was extended; the unloaded PCL solution had a short LVR of between 50 Pa to 100 Pa (shear stress), which then resulted in shear thinning at high shear stresses. These long LVRs are indicative of well-dispersed, stable polymer-drug systems. This behaviour of Newtonian to shear thinning has been previously observed in other studies; it can be attributed to the formation of physical bonding between the drug and the polymer, which causes an increase in the solution viscosity [28].

The frequency sweep data shown in figure 2 are indicative of how the drug dispersed in the matrix affected the overall structure. Again, it was observed that loading the polymer solution with drugs had an effect, with measured viscosity in all three samples appearing to be frequency dependent. According to data in both G’ and G’’ graphs, G’’ was shown to be the dominating effect (G’ ranging from seven to 30 Pa, and G’’ ranging from 150 to 175 Pa). Long regions of viscoelasticity normally imply that there is a certain degree of stability within the polymer matrix; however, the frequency sweep implies otherwise. It appears that G’ and G’’ are both frequency dependent, which implies that the system has little internal network and is easily disturbed [15].

3.2 Fibre Morphology

Figure 3 shows SEM images of the various unloaded and drug-loaded PCL scaffolds. Smooth morphology can be observed in all 3 different scaffolds and at a 12% concentration of polymer, there is no significant beading or any visible signs of either API outside of the fibres. The major differences across the three different scaffolds are the fibre size – the addition of irgasan reduced the average fibre diameter to 1.623 ± 1.9 µm. These fibres appear to be relatively consistent in size compared to other various PCL-fibre studies, 1.1 ± 6.6 µm, 2.7 ± 2.0 µm and 1.83 ± 0.050 µm [9], [29], [30]. The morphology of the levofloxacin-loaded fibres appeared to differ from the unloaded and irgasan loaded fibres: whilst there appears to be a smooth morphology, the fibres appear more densely packed with a greater ‘curvature’ of the fibres. These fibres are also greater in diameter in comparison with the PCL-IRG scaffold, with an average fibre diameter or 2.865 ± 3.0 µm. The PCL-LEVO fibres appear to be much larger in diameter compared with studies by Jalvandi *et al* [12] (600 – 800 nm), Puppi *et al* [31] (219.2 ± 55.1 nm) and Park *et al* [32] (232 ± 20.4 nm). This variation in fibre diameter could possibly be attributed to the higher voltage applied to the target plate during the electrospinning process – for PCL and PCL-IRG solutions, the voltage applied varied between 10 – 12 kV whereas the PCL-LEVO solution was ± 18 kV. There is a critical value of applied voltage, and the increase in the diameter with an increase in the applied voltage are attributed to the decrease in the size of the Taylor cone and increase in the jet velocity for the same flow rate [33].

Considering the morphology of the fibres at a greater detail and image resolution, the AFM characterisation showed a significant difference between the irgasan-loaded and levofloxacin-loaded fibres. Figure 4a shows the smooth morphology of the PCL-IRG scaffold at a 400 nm scale, and it can be clearly seen that there appears to be no signs of API on the surface of the polymer. This suggests that the irgasan is integrated into the polymeric matrix. In contrast, it was found using AFM that within certain areas of the PCL-LEVO scaffold, there appeared to be regions with crystalline API sitting at the surface (figure 4b).

3.3 Surface Characterisation

The CAG results for the irgasan-loaded fibres indicated an increase in the hydrophobicity of the scaffold in comparison to the unloaded PCL scaffold – the water drop took 45 minutes to absorb fully into the PCL-IRG scaffold, and this slow nature of absorption potentially indicates that the irgasan may release in a sustained mechanism. This is most likely due to the hydrophobic nature of irgasan combined within the polymeric matrix of PCL, which also has a certain degree of hydrophobicity. The CAG results for the levofloxacin-loaded scaffolds were inconclusive given that hydrophilic nature of levofloxacin- the water droplet applied was absorbed almost immediately; therefore, no data could be obtained. However, this does support the hypothesis that there may be an amount of levofloxacin sitting at the surface of the sample – the quick absorbance of the water droplet may be the levofloxacin uptake.

3.4 Drug Efficacy of Electrospun Scaffolds

The release of irgasan (figure 5) from the PCL-irgasan scaffold appeared to exhibit sustained release behaviour of the encapsulated drug. The final cumulative drug release was found to be at 50 %; although more irgasan will be released beyond 200 h (equilibrium had not been observed at the 200 hr). The behaviour of the PCL-levofloxacin scaffold was entirely different to the irgasan-loaded scaffold. It exhibited burst release behaviour and the antibiotic was almost entirely lost from the matrix within the first 15 min of measurements.. The final cumulative drug release was also found to be at 50 %. This burst release behaviour is consistent with the manner in which the drug is associated with the polymer matrix – the previous SEM and AFM were indicative of the presence of levofloxacin on the surface of the fibres in some areas.

Determining the drug release profiles of the drugs was a crucial part of this study, as divergent behaviours helped us to characterise bridging properties indicating the manner in which irgasan and levofloxacin dispersed within the polymer matrix. The irgasan released steadily over 145 hours, which would suggest that the drug is being released through molecular diffusion [34]. The levofloxacin exhibited a burst release mechanism, although this may be attributed to the mechanism in which levofloxacin functions in most polymers [32], due to the way the drug is adsorbed on to the surface of the polymer [31], [35].

The main factors that could be expected to influence the drug release kinetics in this study can be summarised as follows are:

- Material matrix: this includes the composition, structure and degradation of polymer; however, the polymer showed no signs of degradation and is known to show a high degree of stability.
- Release medium: the irgasan was released in a buffer of PBS and sodium dodecyl sulphate (surfactant), therefore it could be suggested either that the surfactant is interacting with the polymer/drug or that it is changing the ionic strength of the buffer [36].
- Drug compounds: Fu and Kao [34] cite solubility, stability charges and interaction with matrix as major factors with the drug that may affect the drug release kinetics. The results in our studies can demonstrate this, given that potential charges of the drug were affecting fabrication, therefore it can be assumed that the charges of irgasan and levofloxacin may be affecting the drug release kinetics.

3.5 In-Vitro Antibacterial Activity

The antibacterial efficacy (Figure 6) of both irgasan and levofloxacin-loaded scaffolds were tested against strains of *E. coli* and *S. aureus*, with the efficacy specifically determined by visual zones of inhibition on the agar plate. The PCL-irgasan scaffold showed signs of some activity, albeit weak, against *E. coli* with an average inhibition zone diameter of 0.7 ± 0.5 cm. However, the irgasan-loaded scaffold was particularly successful inhibiting the growth of *S. aureus* with an average inhibition zone diameter of 1.8 ± 0.5 cm. There was a higher-level efficacy observed within the PCL-levofloxacin cultures of both *E. coli* and *S. aureus*. Both strains of bacteria were inhibited on the agar plate with an average diameter of no growth of 2.6 cm. The antibacterial studies have shown that there is a high efficacy of bacteria inhibition in both irgasan and levofloxacin-loaded scaffolds across *E. coli* and *S. aureus* bacteria. The levofloxacin-loaded scaffolds demonstrated larger values of inhibition zones, for both bacteria – this should be the case, given that levofloxacin is a broad-spectrum antibiotic, active against both gram positive and gram negative. The irgasan-loaded scaffold showed stronger inhibition to the *S. aureus* bacteria; however, this should not be viewed as a negative result. *S. aureus* is a gram-positive bacterium that is commonly found on the skin, therefore is a major cause of nosocomial wound infection [37]. The hydrophobic natures of irgasan and PCL, and potential stronger interactions between drug and polymer are likely to aid the sustained release from the fibres – this sustained release can be observed in the previous *in vitro* drug release study, and observed in the reduced inhibition of *E. Coli* [9].

3.6 ToF-SIMS Analysis

Imaging and 3D imaging techniques showed a difference in the distribution of the active pharmaceutical ingredients (API) between Irgasan-loaded and Levofloxacin-loaded fibres. PCL is identified by the ion at *m/z* 113 ($[C_6H_9O_2]^-$ [M-H]$^-$), Levofloxacin by the ions at *m/z* 360 ($[C_{18}H_{19}FN_3O_4]^-$ [M-H]$^-$) and *m/z* 316 ($[C_{17}H_{19}FN_3O_2]^-$), and Irgasan by the ions at *m/z* 287 ($[C_{12}H_6{}^{35}Cl_3O_2]^-$ [M-H]$^-$), *m/z* 289 ($[C_{12}H_6{}^{35}Cl_2{}^{37}Cl_1O_2]^-$) and *m/z* 291 ($[C_{12}H_6{}^{35}Cl_1{}^{37}Cl_2O_2]^-$). The total ion images and the overlays of single ion images for the characteristic peaks of PCL (grey) and the two drugs (yellow) are reported in Figure 7. The ion images show a homogeneous distribution of Irgasan, throughout the electrospun fibres, whilst the Levofloxacin appears to be concentrated in several small areas. This was confirmed by 3D imaging, where Irgasan characteristic peaks appeared to be homogeneously distributed in the volume (Figure 8a). Conversely, Levofloxacin had an intense signal localized to small areas and mainly on the surface (Figure 8b).

4. Conclusions

The purpose of this study was to fabricate drug-loaded fibres that may potentially be used within a hernia repair context. The good understanding of the relationship between the solution viscosity and the spinning parameters is essential if the technique is to be effective, hence the need to characterise the effect of drug loading on the rheological behaviour of the spinning solutions. It was observed that the addition of both irgasan and levofloxacin had a direct influence on the rheological behaviour of the solutions; a reduction in elastic modulus, viscous modulus, and shear viscosity occurred, which may cause a reduction in polymer chain entanglements. However, this explanation may not be the only viable one – rheological behaviour of drug-loaded solutions has been widely researched, although further characterisation into the molecular interactions between drug and polymer may give further insight into why the solution behaviour changes significantly. Atomic force microscopy indicated that crystals, probably of levofloxacin were present on the surface of the polymer fibres, and this was crucial in explaining the behaviour of the drug during *in vivo* release studies and antibacterial activity profile. The presence of levofloxacin at the surface of the polymer was confirmed through contact angle goniometry (immediate absorbance of the water droplet showed the hydrophilic nature of levofloxacin in action), *in vitro* release studies (the drug demonstrated a burst release behaviour), antibacterial studies (an increased average inhibition zone repelled both bacteria types immediately) and ToF-SIMS. In the ToF-SIMS study, the molecular weight of levofloxacin was shown at various areas across the fibres and the 3D imaging of the matrix indicated there was a certain degree of drug encapsulation. This study has contrasted the incorporation of two different drugs within an electrospun fibre, and shown that through bridging chemical, mechanical and biological studies, their behaviours can be fully interpreted. The next stages of this research are to now assess whether these constructs are useful within any clinical scenario, and in particular, within the treatment of hernia repair.

Acknowledgements

The authors would like to thank the UK Engineering & Physical Sciences Research Council (EPSRC) Doctoral Training Centre in Medical Devices, University of Strathclyde (EPSRC Grant Ref. EP/F50036X/1) for the studentship awarded to IHB. The authors would also like to thank the EPSRC Centre in Continuous Manufacturing and Crystallisation (CMAC) for access to specialised instruments.

References

[1] D. B. Earle, “Biomaterials in Hernia Repair,” 2010. [Online]. Available: http://laparoscopy.blogs.com/prevention_management _3/2010/08/biomaterials-in-hernia-repair.html. [Accessed: 15-Sep-2015].

[2] L. Procter, E. E. Falco, J. P. Fisher, and J. S. Roth, “Abdominal Wall Hernias & Biomaterials,” in *Bioengeering Research of Chronic Wounds*, 1st ed., A. Gefen, Ed. Berlin: Springer Verlag, 2009, pp. 425–447.

[3] D. Li, G. Guo, R. Fan, J. Liang, X. Deng, F. Luo, and Z. Qian, “PLA/F68/Dexamethasone implants prepared by hot-melt extrusion for controlled release of anti-inflammatory drug to implantable medical devices: I. Preparation, characterization and hydrolytic degradation study,” *Int. J. Pharm.*, vol. 441, no. 1–2, pp. 365–372, 2013.

[4] A. Toncheva, D. Paneva, N. Manolova, and I. Rashkov, “Electrospun poly(L-lactide) membranes containing a single drug or multiple drug system for antimicrobial wound dressings,” *Macromol. Res.*, vol. 19, no. 12, pp. 1310–1319, 2011.

[5] J. Holländer, N. Genina, H. Jukarainen, M. Khajeheian, A. Rosling, E. Mäkilä, and N. Sandler, “Three-Dimensional Printed PCL-Based Implantable Prototypes of Medical Devices for Controlled Drug Delivery,” *J. Pharm. Jenny, Natalja Genina, Harri Jukarainen, Mohammad Khajeheian, Ari Rosl. Ermei Mäkilä, Niklas Sandler. “Three-Dimensional Print. PCL-Based Implant. Prototypes Med. Devices Control. Drug Deliv. J*, vol. 105, 2016.

[6] I. Sebe, B. Szabo, Z. K. Nagy, D. Szabo, L. Zsidai, B. Kocsis, and R. Zelko, “Polymer structure and antimicrobial activity of polyvinylpyrrolidone-based iodine nanofibres

prepared with high-speed rotary spinning technique," *Int. J. Pharm.*, vol. 458, no. 1, pp. 99–103, 2013.

[7] M. Zamani, M. P. Prabhakaran, and S. Ramakrishna, "Advances in drug delivery via electrospun and electrosprayed nanomaterials," *Int. J. Nanomedicine*, vol. 8, pp. 2997–3017, 2013.

[8] M. He, J. Xue, H. Geng, H. Gu, D. Chen, R. Shi, and L. Zhang, "Fibrous guided tissue regeneration membrane loaded with anti-inflammatory agent prepared by coaxial electrospinning for the purpose of controlled release," *Appl. Surf. Sci.*, vol. 335, pp. 121–129, 2015.

[9] A. Celebioglu, O. C. O. Umu, T. Tekinay, and T. Uyar, "Antibacterial electrospun nanofibers from triclosan/cyclodextrin inclusion complexes," *Colloids Surfaces B Biointerfaces*, vol. 116, pp. 612–619, 2014.

[10] O. Hartman, C. Zhang, E. L. Adams, M. C. Farach-carson, J. Petrelli, B. D. Chase, and J. F. Rabolt, "Biofunctionalization of electrospun PCL-based scaffolds with perlecan domain IV peptide to create a 3-D pharmacokinetic cancer model," *Biomaterials*, vol. 31, no. 21, pp. 5700–5718, 2011.

[11] G. Kabay, G. Kaleli, Z. Sultanova, T. T. Ölmez, U. Ö. Ş. Şeker, and M. Mutlu, "Biocatalytic protein membranes fabricated by electrospinning," *React. Funct. Polym.*, vol. 103, pp. 26–32, 2016.

[12] J. Jalvandi, M. White, Y. B. Truong, Y. Gao, R. Padhye, and I. L. Kyratzis, "Release and antimicrobial activity of levofloxacin from composite mats of poly(e-caprolactone) and mesoporous silica nanoparticles fabricated by core-shell electrospinning," *J. Mater. Sci.*, vol. 50, no. 24, pp. 7967–7974, 2015.

[13] A. S. Goldstein and P. S. Thayer, “Fabrication of complex biomaterial scaffolds for soft tissue engineering by electrospinning,” in *Nanobiomaterials in Soft Tissue Engineering*, A. Grumezescu, Ed. Amsterdam: William Andrew, 2016, pp. 299–330.

[14] S. Agarwal and A. Greiner, “On the way to clean and safe electrospinning-green electrospinning: Emulsion and suspension electrospinning,” *Polym. Adv. Technol.*, vol. 22, no. 3, pp. 372–378, 2011.

[15] K. Bubel, D. Grunenberg, G. Vasilyev, E. Zussman, S. Agarwal, and A. Greiner, “Solvent-Free Aqueous Dispersions of Block Copolyesters for Electrospinning of Biodegradable Nonwoven Mats for Biomedical Applications,” *Macromol. Mater. Eng.*, pp. 1445–1454, 2014.

[16] M. D. Bhavsar and M. M. Amiji, “Development of novel biodegradable polymeric nanoparticles-in-microsphere formulation for local plasmid DNA delivery in the gastrointestinal tract.,” *AAPS PharmSciTech*, vol. 9, no. 1, pp. 288–94, 2008.

[17] B. Azimi, P. Nourpanah, M. Rabiee, and S. Arbab, “Poly (lactide -co- glycolide) Fiber : An Overview.”

[18] D. N. Bikiaris, G. Z. Papageorgiou, D. S. Achilias, E. Pavlidou, and A. Stergiou, “Miscibility and enzymatic degradation studies of poly(ε-caprolactone)/poly(propylene succinate) blends,” *Eur. Polym. J.*, vol. 43, no. 6, pp. 2491–2503, 2007.

[19] R. S. R. Murthy, “Biodegradable Polymers,” N. K. Jain, Ed. New Dehli: CBS Publisher, 1997, pp. 27–51.

[20] G. C. Ebersole, E. G. Buettmann, M. R. MacEwan, M. E. Tang, M. M. Frisella, B. D. Matthews, and C. R. Deeken, “Development of novel electrospun absorbable polycaprolactone (PCL) scaffolds for hernia repair applications,” *Surg. Endosc. Other*

Interv. Tech., vol. 26, no. 10, pp. 2717–2728, 2012.

[21] D. A. Lamprou, V. Venkatpurwar, and M. N. V. R. Kumar, “Atomic Force Microscopy Images Label-Free, Drug Encapsulated Nanoparticles In Vivo and Detects Difference in Tissue Mechanical Properties of Treated and Untreated: A Tip for Nanotoxicology,” *PLoS One*, vol. 8, no. 5, pp. 8–12, 2013.

[22] D. A. Lamprou, J. R. Smith, T. G. Nevell, E. Barbu, C. R. Willis, and J. Tsibouklis, “Self-assembled structures of alkanethiols on gold-coated cantilever tips and substrates for atomic force microscopy: Molecular organisation and conditions for reproducible deposition,” *Appl. Surf. Sci.*, vol. 256, no. 6, pp. 1961–1968, 2010.

[23] K. DUAN, D. XIAO, and J. WENG, “Triclosan-loaded PLGA microspheres-porous titanium composite coating,” pp. 1–6, 2013.

[24] A. Piccoli, J. Fiori, V. Andrisano, and M. Orioli, “Determination of triclosan in personal health care products by liquid chromatography (HPLC),” *Farmaco*, vol. 57, no. 5, pp. 369–372, 2002.

[25] M. Maleque, M. R. Hasan, F. Hossen, and S. Safi, “Development and validation of a simple UV spectrophotometric method for the determination of levofloxacin both in bulk and marketed dosage formulations,” *J. Pharm. Anal.*, vol. 2, no. 6, pp. 454–457, 2012.

[26] S. M. Davachi, B. Kaffashi, A. Zamanian, B. Torabinejad, and Z. Ziaeirad, “Investigating composite systems based on poly l-lactide and poly l-lactide/triclosan nanoparticles for tissue engineering and medical applications,” *Mater. Sci. Eng. C*, vol. 58, pp. 294–309, 2016.

[27] J. R. Dias, F. E. Antunes, and P. J. Bártolo, “Influence of the rheological behaviour in

electrospun PCL nano fibres production for tissue engineering application," *Chem. Eng. Trans.*, vol. 32, no. 2011, pp. 1015–1020, 2013.

[28] Z. Sadrearhami, M. Morshed, and J. Varshosaz, "Production and evaluation of polyblend of agar and polyacrylonitrile nanofibers for in vitro release of methotrexate in cancer therapy," *Fibers Polym.*, vol. 16, no. 2, pp. 254–262, 2015.

[29] N. Detta, T. D. Brown, F. K. Edin, K. Albrecht, F. Chiellini, E. Chiellini, P. D. Dalton, and D. W. Hutmacher, "Melt electrospinning of polycaprolactone and its blends with poly(ethylene glycol)," *Polym. Int.*, vol. 59, no. 11, pp. 1558–1562, 2010.

[30] L. J. Del Valle, R. Camps, A. Díaz, L. Franco, A. Rodríguez-Galán, and J. Puiggalí, "Electrospinning of polylactide and polycaprolactone mixtures for preparation of materials with tunable drug release properties," *J. Polym. Res.*, vol. 18, no. 6, pp. 1903–1917, 2011.

[31] D. Puppi, D. Dinucci, C. Bartoli, C. Mota, C. Migone, F. Dini, G. Barsotti, F. Carlucci, and F. Chiellini, "Development of 3D wet-spun polymeric scaffolds loaded with antimicrobial agents for bone engineering," *J. Bioact. Compat. Polym.*, vol. 26, pp. 478–492, 2011.

[32] H. Park, H. Yoo, T. Hwang, T. J. Park, D. H. Paik, S. W. Choi, and J. H. Kim, "Fabrication of levofloxacin-loaded nanofibrous scaffolds using coaxial electrospinning," *J. Pharm. Investig.*, vol. 42, no. 2, pp. 89–93, 2012.

[33] A. Haider, S. Haider, and I. K. Kang, "A comprehensive review summarizing the effect of electrospinning parameters and potential applications of nanofibers in biomedical and biotechnology," *Arab. J. Chem.*, 2015.

[34] F. Yao and J. K. Weiyuan, "Drug Release Kinetics and Transport Mechanisms of Non-

degradable and Degradable Polymeric Delivery Systems," *Expert Opin. Drug Deliv.*, vol. 7, no. 4, pp. 429–444, 2010.

[35] W. S. Cheow, M. W. Chang, and K. Hadinoto, "Antibacterial efficacy of inhalable levofloxacin-loaded polymeric nanoparticles against E. coli biofilm cells: The effect of antibiotic release profile," *Pharm. Res.*, vol. 27, no. 8, pp. 1597–1609, 2010.

[36] M. Thongngam and D. J. McClements, "Influence of pH, ionic strength, and temperature on self-association and interactions of sodium dodecyl sulfate in the absence and presence of chitosan," *Langmuir*, vol. 21, no. 1, pp. 79–86, 2005.

[37] M. Sisirak, A. Zvizdic, and M. Hukic, "Methicillin-resistant *Staphylococcus aureus* (MRSA) as a cause of nosocomial wound infections," *Bosn. J. Basic Med. Sci.*, vol. 10, no. 1, pp. 32–37, 2010.

Figure Captions

Figure 1 a: Amplitude sweep viscous modulus (G') data for PCL, PCL-IRG and PCL-LEVO solutions; **b**: Amplitude sweep viscous modulus (G'') data for PCL, PCL-IRG and PCL-LEVO solutions; **c**: Amplitude sweep shear viscosity (η) data for PCL, PCL-IRG and PCL-LEVO solutions.

Figure 2 a: Frequency sweep elastic modulus (G') data for PCL, PCL-IRG and PCL-LEVO solutions; **b**: Frequency sweep viscous modulus (G'') data for PCL, PCL-IRG and PCL-LEVO solutions; **c**: Frequency sweep shear viscosity (η) data for PCL, PCL-IRG and PCL-LEVO solutions.

Figure 3: SEM images of PCL (a), PCL-IRG (b) and PCL-LEVO (c) electrospun fibres.

Figure 4 a: AFM image of PCL-IRG fibres; **b**: AFM image of PCL-LEVO fibres.

Figure 5: Cumulative drug release percentages for the release of IRG and LEVO in PBS media.

Figure 6: Images showing the average zone of inhibition of PCL-IRG and PCL-LEVO against bacterial strains of *E. coli* and *S. aureus*.

Figure 7a/b: The images above are acquired with a high lateral resolution mode, which enables to easily visualise the nanofibers (total ion image A and B) and the distribution of the API (colour overlay images C and D); **c**: Overlay of $[C_6H_9O_2]^-$ (PCL) in grey and $[C_{12}H_6Cl_3O_2]^-$ (Irgasan) in yellow; **d**: Overlay of $[C_6H_9O_2]^-$ (PCL) in grey and of $[C_{17}H_{19}FN_3O_2]^-$ and $[C_{18}H_{19}FN_3O_4]^-$ (Levofloxacin) in yellow.

Figure 8a: The 2D (left) and 3D images show the distribution of $[C_6H_9O_2]^-$ (PCL) in grey and $[C_{12}H_6Cl_3O_2]^-$ (Irgasan) in yellow. The analysed volume is 100 µm x 100 µm on the X-Y axes, and ~3 µm on the Z axis: (A) viewed from the top and (B) inclined in order to aid 3D visualization.

Figure 8b: The 2D (left) and 3D images show the distribution of $[C_6H_9O_2]^-$ (PCL) in grey and of $[C_{17}H_{19}FN_3O_2]^-$ and $[C_{18}H_{19}FN_3O_4]^-$ (Levofloxacin) in yellow. The analysed volume is 100 µm x 100 µm on the X-Y axes, and ~3 µm on the Z axis: (A) viewed from the top and (B) inclined in order to aid 3D visualization.

Figure 1a.

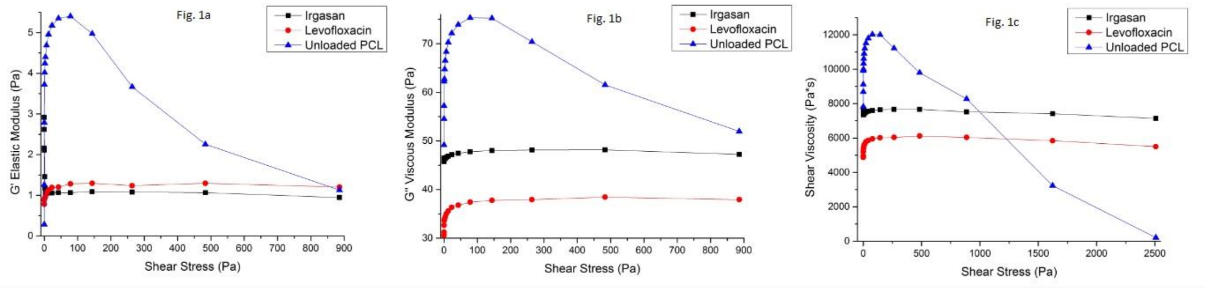
Fig. 1a
Irgasan
Levofloxacin
Unloaded PCL
G' Elastic Modulus (Pa)
0
1
2
3
4
5
0
100
200
300
400
500
600
700
800
900
Shear Stress (Pa)
Fig. 1b
Irgasan
Levofloxacin
Unloaded PCL
G'' Viscous Modulus (Pa)
30
40
50
60
70
0
100
200
300
400
500
600
700
800
900
Shear Stress (Pa)
Fig. 1c
Irgasan
Levofloxacin
Unloaded PCL
Shear Viscosity (Pa*s)
0
2000
4000
6000
8000
10000
12000
0
500
1000
1500
2000
2500
Shear Stress (Pa)

Figure 2.

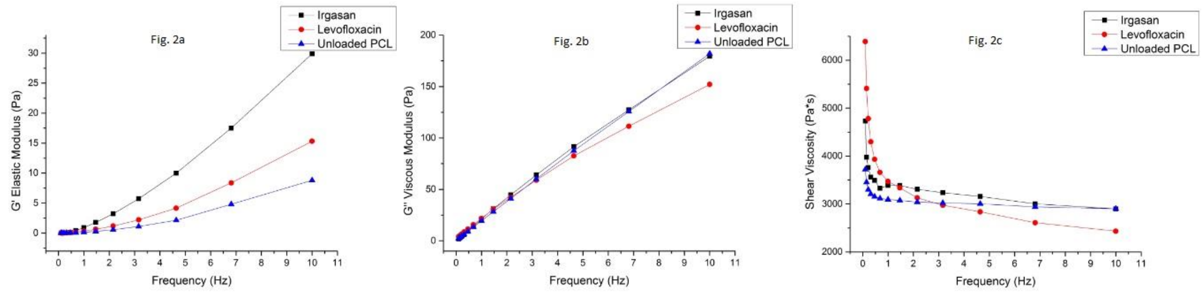
Fig. 2a
Irgasan
Levofloxacin
Unloaded PCL
G' Elastic Modulus (Pa)
0
5
10
15
20
25
30
Frequency (Hz)
0
1
2
3
4
5
6
7
8
9
10
11
Fig. 2b
Irgasan
Levofloxacin
Unloaded PCL
G'' Viscous Modulus (Pa)
0
50
100
150
200
Frequency (Hz)
0
1
2
3
4
5
6
7
8
9
10
11
Fig. 2c
Irgasan
Levofloxacin
Unloaded PCL
Shear Viscosity (Pa*s)
2000
3000
4000
5000
6000
Frequency (Hz)
0
1
2
3
4
5
6
7
8
9
10
11

Figure 3.

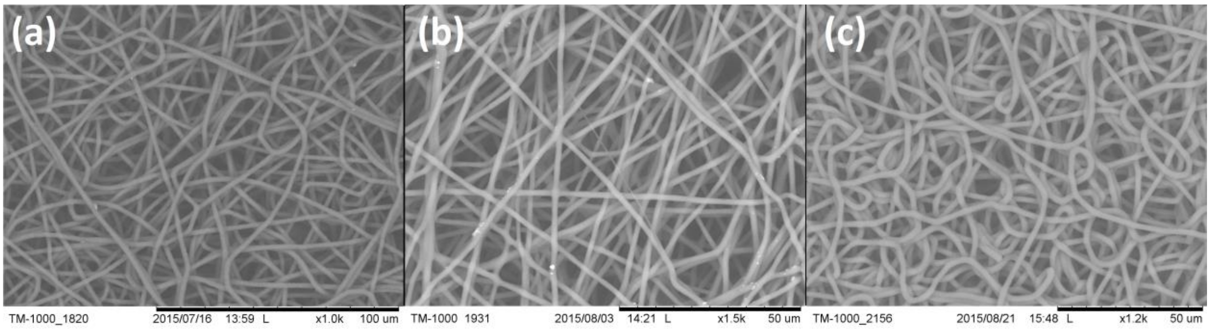
(a)
(b)
(c)
TM-1000_1820 2015/07/16 13:59 L x1.0k 100 um
TM-1000 1931 2015/08/03 14:21 L x1.5k 50 um
TM-1000_2156 2015/08/21 15:48 L x1.2k 50 um

Figure 4.

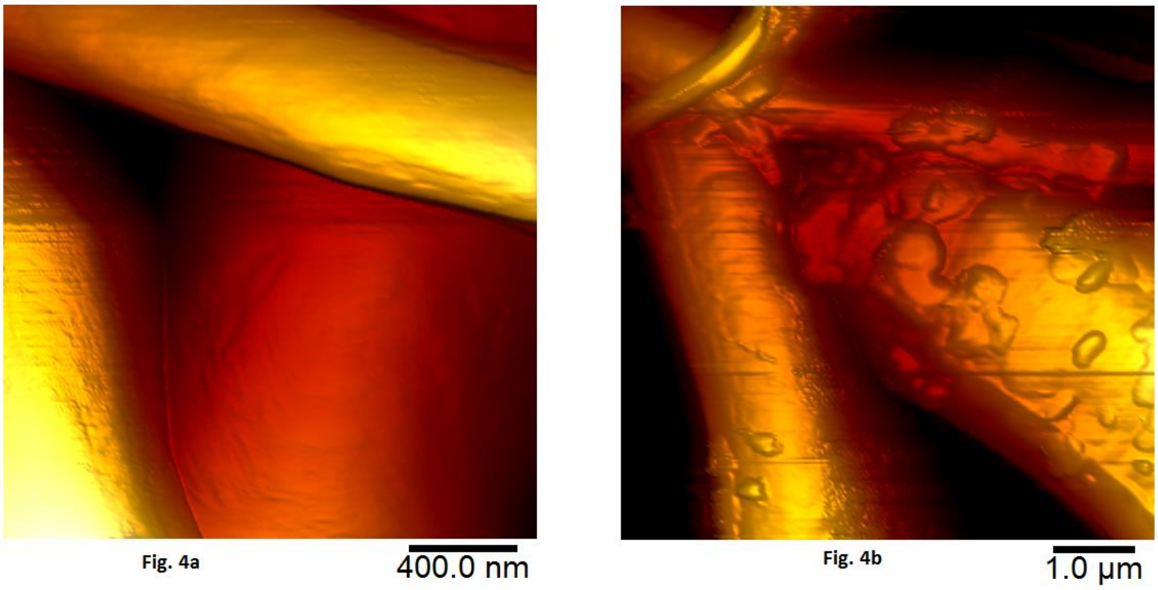

Fig. 4a

Fig. 4b

Figure 5.

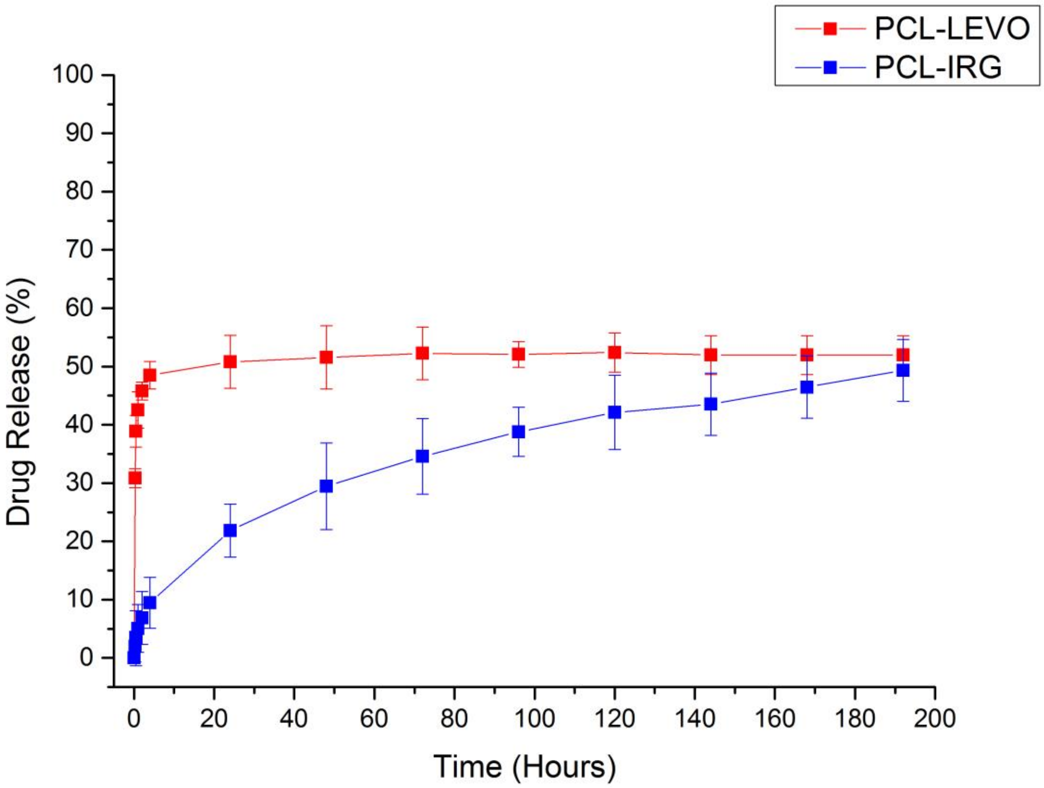
PCL-LEVO
PCL-IRG
Drug Release (%)
0
10
20
30
40
50
60
70
80
90
100
Time (Hours)
0
20
40
60
80
100
120
140
160
180
200

Figure 6.

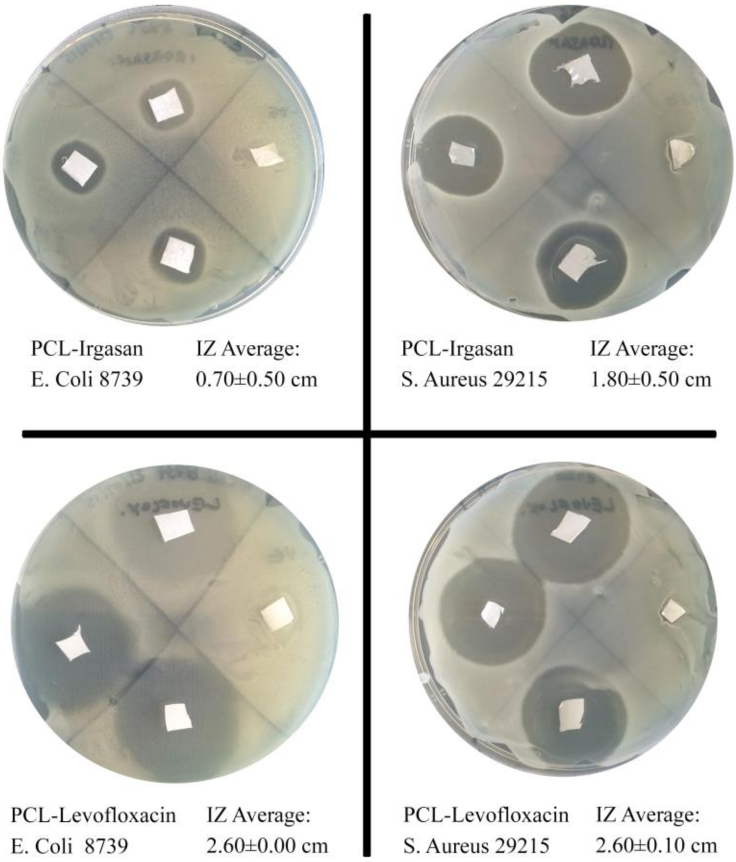
PCL-Irgasan
E. Coli 8739
IZ Average:
0.70±0.50 cm
PCL-Irgasan
S. Aureus 29215
IZ Average:
1.80±0.50 cm
PCL-Levofloxacin
E. Coli 8739
IZ Average:
2.60±0.00 cm
PCL-Levofloxacin
S. Aureus 29215
IZ Average:
2.60±0.10 cm

Figure 7.

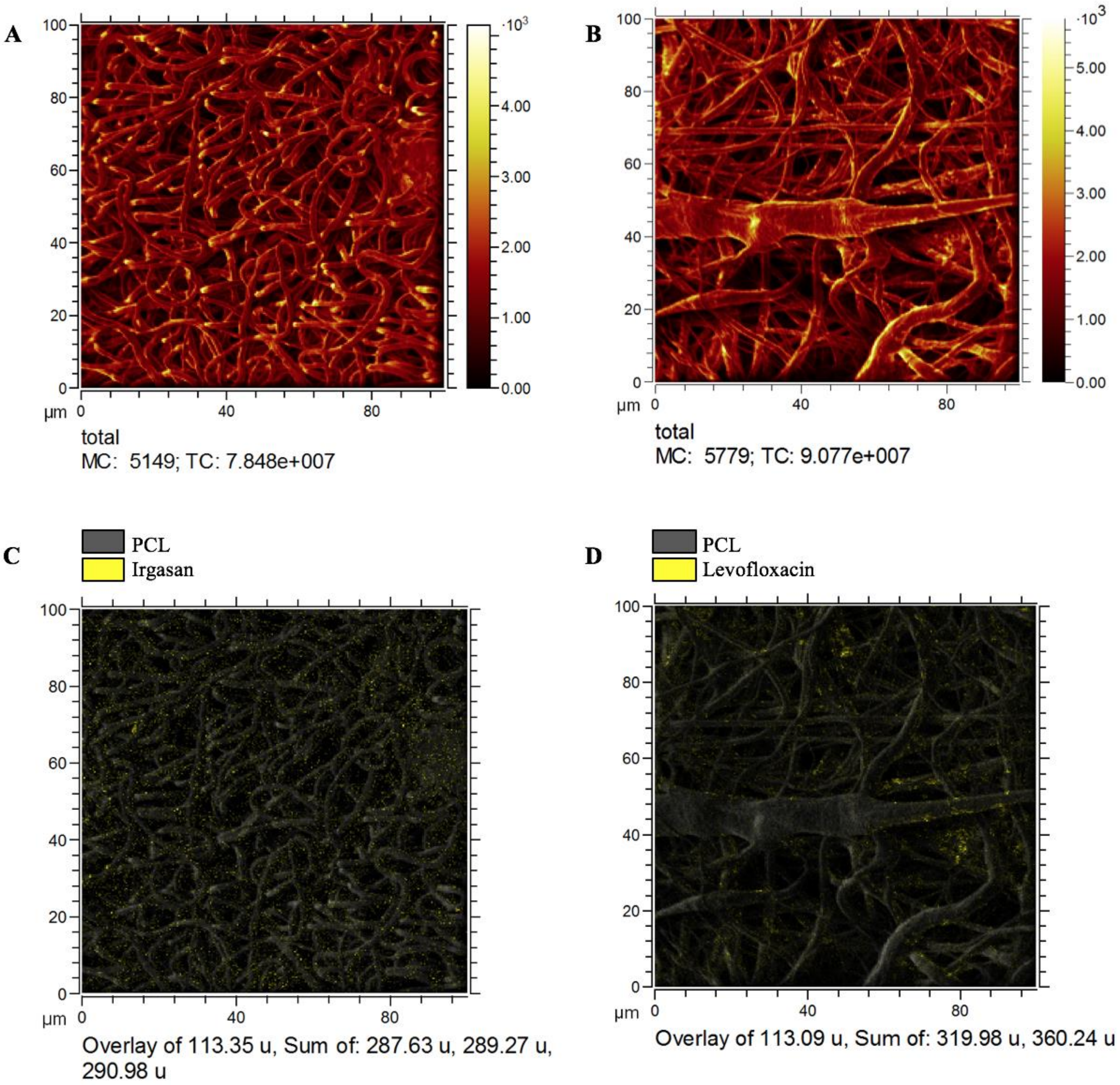
A
100
80
60
40
20
0
µm 0
40
80
·10³
4.00
3.00
2.00
1.00
0.00
total
MC: 5149; TC: 7.848e+007
B
·10³
5.00
4.00
3.00
2.00
1.00
0.00
total
MC: 5779; TC: 9.077e+007
C
PCL
Irgasan
Overlay of 113.35 u, Sum of: 287.63 u, 289.27 u, 290.98 u
D
PCL
Levofloxacin
Overlay of 113.09 u, Sum of: 319.98 u, 360.24 u

Figure 8a.

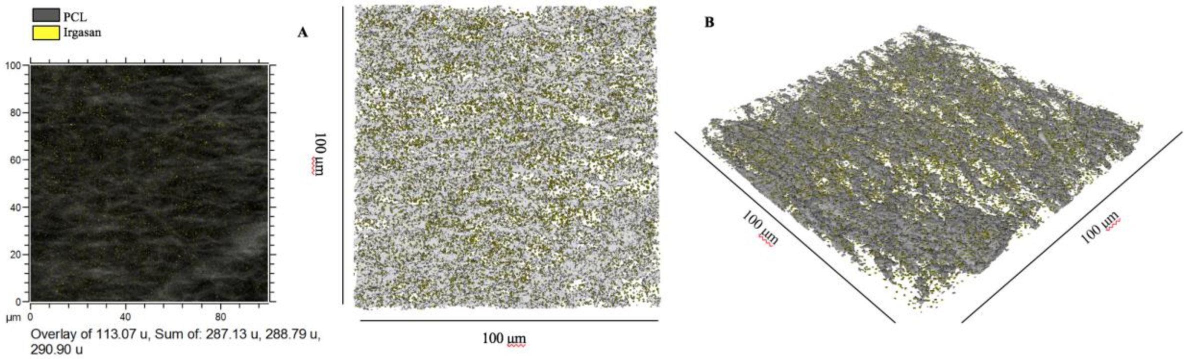

Figure 8b.

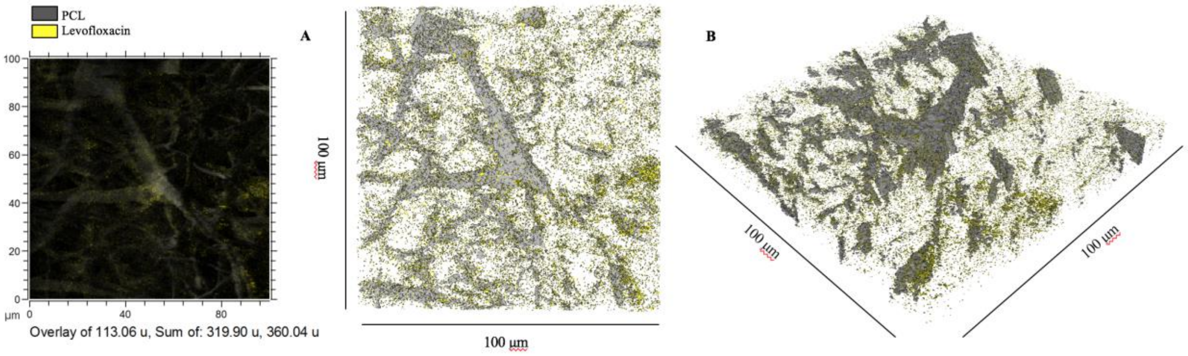

.